*International Journal of Minerals, Metallurgy and Materials*
*Volume 23, Number 11, November 2016, Page 1340*
**DOI: 10.1007/s12613-016-1356-3**

# Characterization and photoluminescence properties of ultrafine copper molybdate (α-$CuMoO_4$) powders prepared via a combustion-like process

*Mohamed Benchikhi*[1, 2)], *Rachida El Ouatib*[1)], *Sophie Guillemet-Fritsch*[2)], *Lahcen Er-Rakho*[1)], *and Bernard Durand*[2)]

1) Laboratoire de Physico-Chimie des Matériaux Inorganiques, Faculté des Sciences Ain Chock, Université Hassan II Casablanca, Morocco
2) Institut Carnot CIRIMAT, CNRS Université de Toulouse, 118 route de Narbonne, 31062 Toulouse Cedex 9, France
(Received: 18 May 2016; revised: 25 July 2016; accepted: 29 August 2016)

**Abstract:** We report a simple method for preparing copper(II) molybdate ($CuMoO_4$) powders via a combustion-like process. A gel was first prepared by the polymerizable complex method, where citric acid was used as a complexing and polymerizing agent and nitric acid was used as an oxidizing agent. The thermal decomposition behavior of the (CuMo)-precursor gel was studied by thermogravimetry–differential thermal analysis (TG–DTA), Fourier transform infrared spectroscopy (FTIR), and X-ray diffraction (XRD). We observed that the crystallization of $CuMoO_4$ powder was completed at 450°C. The obtained homogeneous powder was composed of grains with sizes in the range from 150 to 500 nm and exhibited a specific surface area of approximately 5 $m^2/g$. The average grain size increased with increasing annealing temperature. The as-prepared $CuMoO_4$ crystals showed a strong green photoluminescence emission at room temperature under excitation at 290 nm, which we mainly interpreted on the basis of the Jahn–Teller effect on [$MoO_4^{2-}$] complex anions. We also observed that the photoluminescence intensity increased with increasing crystallite size.

**Keywords:** copper molybdate; chemical synthesis; photoluminescence; Jahn–Teller effect

## 1. Introduction

Transition-metal molybdates $AMoO_4$ (A = $Cu^{2+}$, $Ni^{2+}$, $Co^{2+}$, and $Fe^{2+}$) have been extensively studied over the past several decades because of their specific structural, electronic, magnetic, and catalytic properties [1−5]. Among all transition-metal molybdates, copper molybdate is one of the most promising catalysts for the partial oxidation of light alkanes, particularly in the case of propane and isobutene [3−5]. In addition to this oxide's catalytic properties, its other properties, including its thermochromic, tribochromic, piezochromic, and photoelectrochemical properties, make it useful in various applications [5−6]. Copper(II) molybdate ($CuMoO_4$) exhibits two polymorphs at atmospheric pressure: the α form, in which Mo is located in a tetrahedral environment (green), and the γ form, in which Mo is located in an octahedral environment (brown-red) [6−7]. Under standard temperature and pressure conditions, the α → γ transition is induced either by an increase of pressure above 250 MPa or by cooling to less than 200 K [6]. In the case of tungsten-doped copper (II) molybdate, $CuMo_{(1-x)}W_xO_4$ ($x \leq 0.12$), the temperature and the pressure of the transition depend on the tungsten content [8−9]. Thus, $CuMoO_4$ can be used as a pressure and/or temperature sensor.

The most general method used to prepare $CuMoO_4$ involves a solid-state reaction between copper and molybdenum oxides at temperatures near 750°C. However, $CuMoO_4$ powders tend to contain relatively large particles with an inhomogeneous composition [6−7]. These problems can be solved through the use of wet-chemical synthesis methods such as co-precipitation [10], spray pyrolysis technique [11], polymeric precursor method [12], and hydrothermal method [13]; these approaches offer the possibility of preparing highly pure and homogeneous ultrafine ceramic powders.

Corresponding author: Mohamed Benchikhi E-mail: Benchikhi_mohamed@yahoo.fr

The metal molybdates generally exhibit blue or green luminescence emission, which is commonly attributed to charge-transfer transitions into the [$MoO_4^{2-}$] tetrahedron [14–20]. However, to the best of our knowledge, the photoluminescence of $CuMoO_4$ crystals has not yet been reported. This work describes the synthesis of ultrafine copper(II) molybdate (α-$CuMoO_4$) powders by a combustion-like process. The main advantage of this synthesis method lies in the chemical homogeneity of the obtained powders and in the control of the particle size [16, 21–22]. A redox reaction between nitrate ions and citrate ions liberates the required energy to synthesize the oxide powder at low temperatures [23]. Furthermore, the optical properties of the synthesized $CuMoO_4$ powders were investigated on the basis of their photoluminescence (PL) emission spectra.

## 2. Experimental

The following reactants were used as raw materials: copper(II) oxide (CuO, Acros Organics, 99.0%), molybdenum(VI) oxide ($MoO_3$, Acros Organics, 99.0%), citric acid (CA, Acros Organics, 99.0%), concentrated nitric acid, and aqueous ammonia. Initially, the $MoO_3$ and CuO were dissolved in an ammonia solution (2 M) and in a nitric acid solution (2 M), respectively. A CA solution was added to an equimolar solution of metal ions in a proportion such that the CA/cation was 3. The solutions were mixed and adjusted to pH 1 using aqueous $NH_4OH$ or $HNO_3$. The resulting mixture was well stirred for 30 min at 50–60°C to produce a homogeneous solution. The evaporation of the solution at 100°C led to the formation of gels. These CuMo gels were dried at 120°C for 24 h and then pre-calcined at 300°C in air for 12 h. The resulting black powders were treated under air at temperatures ranging from 450 to 550°C.

The crystallization process of the (CuMo)-precursor gel was evaluated by thermogravimetry–differential thermal analysis (TG–DTA, SETERAM TG-DTA 92) and Fourier transform infrared spectroscopy (FTIR, Perkin Elmer 1760) using the KBr pellet technique. The phase after the heat treatment was identified by X-ray diffraction (Bruker AXSD4, Cu $K_\alpha$, $\lambda$ = 0.154056 nm, operating voltage 40 kV and current 40 mA) with a 0.02° step scan and a count time of 3.6 s/step. The size and morphology of the green powders were studied by scanning (Jeol JSM6400 equipped with energy-dispersive X-ray spectrometer) and transmission (Jeol 2010) electron microscopies. Specific surface areas were determined using a Micrometrics Flowsorb II 2300. The PL spectra were recorded at room temperature using a Hamamatsu S20 photocathode ($\lambda$ = 290 nm).

## 3. Results and discussion

### 3.1. Synthesis of $CuMoO_4$ ultrafine powders

The crystallization process of the (CuMo)-precursor gel was evaluated by TG–DTA, FTIR, and X-ray diffraction (XRD). Fig. 1 shows the typical thermal behavior of a dried gel, as evaluated in air at a heating rate of 2.5°C/min. The TG curve reveals that the CuMo-gel loses mass as the temperature is increased to 450°C. With a further increase in temperature, the mass remains constant, indicating that the decomposition of all organic materials was accomplished below 450°C. The DTA curve shows a single endothermic peak and several exothermic peaks between 200 and 450°C. The broad endothermic peak at 140–150°C is attributed to the evaporation of free water and adsorbed water; this attribution is confirmed by the mass loss in the TG graph. The distinct exothermic peaks at 200–360°C in the DTA curve are attributed to the decomposition of citrates, nitrates, and ammonium groups and to the nucleation of metal oxides. This nucleation is accompanied by a drastic mass loss in the TG curve. The exothermic peak at 410–415°C with weak mass loss in the TG curve is ascribed to the complete oxidation of residual carbon in the powder and to the crystallization of $CuMoO_4$.

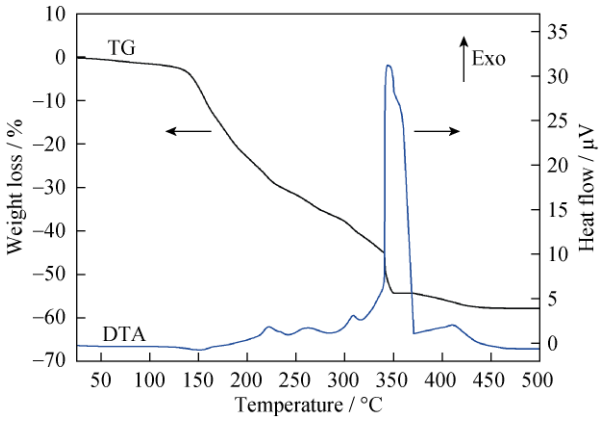


**Fig. 1. Simultaneous TG–DTA curves of a dried (CuMo)-gel under flowing air.**

The FTIR spectra of the powders heat-treated between 120 and 450°C are shown in Fig. 2. The FTIR spectrum of the gel dried at 120°C shows bands at approximately 3430 and 1720 $cm^{-1}$, corresponding to the O–H and C=O stretching modes, respectively [24]. The IR peaks observed at 1400 and 1630 $cm^{-1}$ are due to the symmetric and asymmetric stretching vibrations of C=O bonds in metal carboxylates; the appearance of these peaks confirms the formation of the metal–citrate complex [25–26]. The observed peak at 1380 $cm^{-1}$ is due to the symmetric deformation of $NH_4^+$ ions [27].

The disappearance or decrease of these bands in the FTIR spectra of the powders heat-treated between 300 and 450°C is a consequence of the pyrolysis of the organic species. In the case of the sample heated at 450°C, numerous peaks (966, 946, 907, 873, 846, 823, 797, 744, 728, and 496 $cm^{-1}$) were observed in its FTIR spectrum. All these bands are attributable to the vibrational modes of $CuMoO_4$ [28], suggests that $CuMoO_4$ was formed before 450°C, consistent with the TG–DTA results.

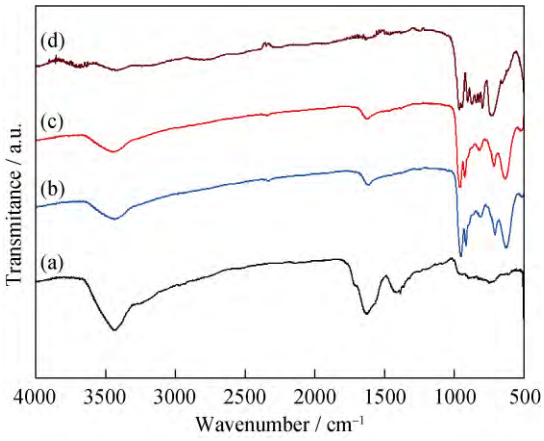


**Fig. 2. FTIR spectra of (CuMo)-gel annealed at (a) 120, (b) 300, (c) 420, and (d) 450°C.**

Fig. 3 shows the XRD patterns of the $CuMoO_4$ powders heat-treated at different temperatures. In the pattern of the powder heat-treated at 300°C (Fig. 3(a)), three phases were identified: α-$CuMoO_4$ (JCPDS 073-0488), $MoO_3$ (JCPDS 076-1003), and $Cu_2MoO_5$ (ICDD 022-0607). The phase α-$CuMoO_4$ was preponderant, and the peaks of the additional phases were very weak in the sample annealed at 420°C (Fig. 3(b)). The diffractogram of the powder heat-treated at 450–550°C (Figs. 3(c)–3(e)) shows only peaks characteristic of the α-$CuMoO_4$ phase. These results are in perfect agreement with TG–DTA and FTIR results.

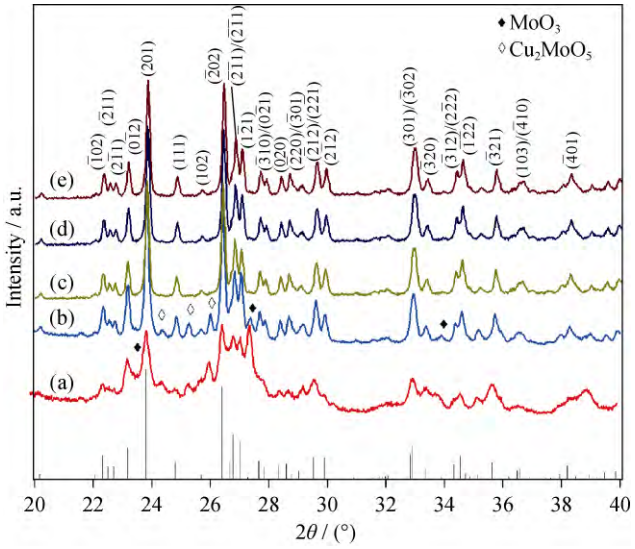


**Fig. 3. XRD patterns of $CuMoO_4$ powders heat-treated at (a) 300, (b) 420, (c) 450, (d) 500, and (e) 550°C for 6 h. The standard pattern for $CuMoO_4$ (JCPDS file No. 73-0488) is provided at the bottom of this figure.**

SEM observation of the powders heat-treated at 450, 500, and 550°C reveals highly agglomerated particles with a polydisperse size distribution (Fig. 4). The size of the agglomerates increases with increasing temperature. The average grain sizes of the powders heat-treated at 450–550°C were measured using transmission electron microscopy (TEM, Table 1). A TEM micrograph of the $CuMoO_4$ powder heat-treated at 450°C is presented as a typical example (Fig. 5). The sample consists of elongated or more-or-less spherical elementary grains with sizes in the range from 150 to 500 nm. As the annealing temperature is increased, the grain size increases, as shown in Table 1. The specific surface area of these powders decreases with increasing calcination temperature (Table 1), which confirms the microscopic observations.

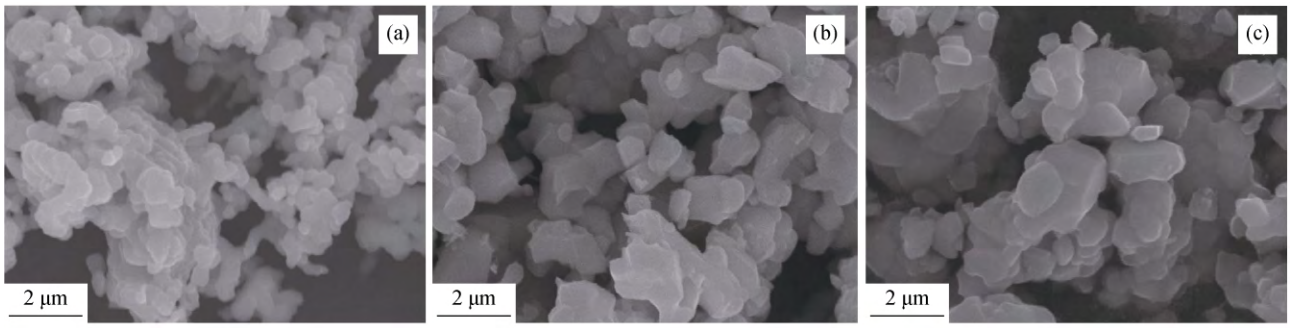


**Fig. 4. SEM micrographs of $CuMoO_4$ powders heat-treated at (a) 450, (b) 500, and (c) 550°C for 6 h.**

The geometrical sizes of particles (calculated from the experimental specific surface area values under the assumption that the powders are composed of monodispersed spherical grains) and the sizes of grains measured on TEM

images were of the same order of magnitude (Table 1). The Cu/Mo molar ratio determined by energy-dispersive X-ray spectroscopy (EDX) is approximately 0.99, which is similar to the stoichiometric composition of $CuMoO_4$.

**Table 1. Calculated average grain size of $CuMoO_4$ as a function of heating temperature**

| Temperature / °C | $D^a_{TEM}$ / μm | $S_{BET}$ / ($m^2 \cdot g^{-1}$) | $D^b_{BET}$ / μm |
|---|---|---|---|
| 450 | 0.15–0.50 | 4.95 | 0.281 |
| 500 | 0.20–0.60 | 4.17 | 0.334 |
| 550 | 0.40–1.60 | 3.50 | 0.397 |

Note: [a] Size of particles estimated by TEM. [b] Geometrical size of particles calculated from the specific surface area ($S_{BET}$) according to the formula $D_{BET} = 6/(dS_{BET})$, where $d$ is the density of $CuMoO_4$.

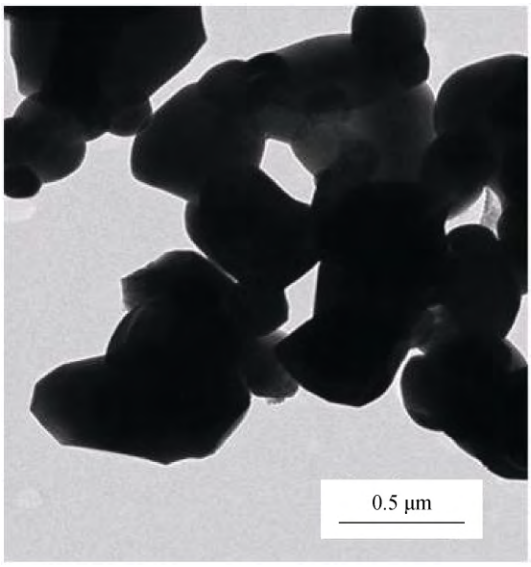


**Fig. 5. TEM micrograph of $CuMoO_4$ powders heat-treated at 450°C for 6 h.**

### 3.2. Photoluminescence properties

Fig. 6 presents the PL emission spectra of the $CuMoO_4$ crystals heat-treated at different temperatures. The sample heat-treated at 450°C shows a broad greenish-blue emission peak at 475–575 nm, whereas samples treated at 500 and 550°C exhibit a PL emission in the green wavelength range, with a maximum at 530–590 nm. The small shoulders observed in the PL spectrum of the sample heat-treated at 450°C can be interpreted as extrinsic transitions induced by structural defects [14]. The PL intensity increases with increasing temperature. These results reveal that the PL emission of $CuMoO_4$ is strongly dependent on its crystallinity.

Various authors have reported that the optical properties of inorganic powders depend on their morphology and crystallite size. Lim [15] has shown that the PL intensity of $(Ba,Ca)MoO_4$ particles depends strongly on their particle shape and distribution; similar observations have been reported previously [16–18]. The PL spectra of $CuMoO_4$ are very similar to those of other bivalent metal molybdates [17–18]. According to the literature, the blue emission of the metal molybdates is mainly attributable to the charge-transfer transitions localized at the $[MoO_4^{2-}]$ tetrahedra [15–19]. Wu *et al.* [19] argued that the blue PL emission is due to a $^1T_2 \rightarrow {}^1A_1$ transition in the tetrahedral molybdate groups. Another possible explanation for the PL emission processes of copper molybdates is the Jahn-Teller splitting effect on excited states of tetrahedral $[MoO_4^{2-}]$ anions. Campos *et al.* [20] showed that the greenish-blue PL emission processes of lead molybdates can be related to the existence of distorted $[MoO_4^{2-}]$ complex clusters into the lattice. Therefore, we attributed the greenish-blue PL emission of copper molybdate to the intrinsic slightly distorted $[MoO_4^{2-}]$ tetrahedra.

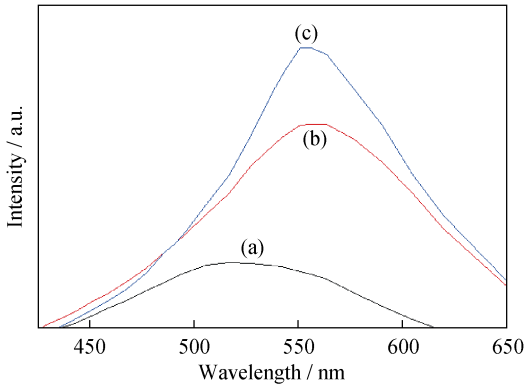


**Fig. 6. PL spectra at room temperature of the $CuMoO_4$ crystals excited at 290 nm after heat treatment at (a) 450, (b) 500, and (c) 550°C.**

## 4. Conclusion

α-$CuMoO_4$ submicronic powders were prepared via a combustion-like process. Crystallization of the $CuMoO_4$ precursor was detected at a relatively low temperature of 300°C and was entirely completed at 450°C. The $CuMoO_4$ powders heat-treated at 450°C are composed of grains with sizes in the range from 150 to 500 nm and exhibit a specific surface area of approximately 5 $m^2/g$. EDX analysis confirmed that the composition of the powder was similar to the stoichiometry of $CuMoO_4$. The powdered $CuMoO_4$ exhibited a broad peak in the green and blue wavelength ranges, which we explained by the influence of the Jahn-Teller effect on nearly tetrahedral $[MoO_4^{2-}]$ groups. The enhancement of PL intensity with increasing calcination temperature was due to the improvement of the crystallinity of $CuMoO_4$.

## Acknowledgements

This work was supported by two French–Moroccan projects: Volubilis Partenariat Hubert Curien (PHC No. MA 09 205) and Projet de Recherches Convention Internationale du CNRS (CNRS-CNRST No. w22572).

## References

[1] H. Ehrenberg, M. Wiesmann, J. Garcia-Jaca, H. Weitzel, and H. Fuess, Magnetic structures of the high-pressure modifications of $CoMoO_4$ and $CuMoO_4$, *J. Magn. Magn. Mater.*, 182(1989), No. 1-2, p. 152.

[2] J.H. Ryu, S.M. Koo, J.W. Yoon, C.S. Lim, and K.B. Shim, Synthesis of nanocrystalline $MMoO_4$ (M=Ni, Zn) phosphors via a citrate complex route assisted by microwave irradiation and their photoluminescence, *Mater. Lett.*, 60(2006), No. 13-14, p. 1702.

[3] L.A. Palacio, A. Echavarría, L. Sierra, and E.A. Lombardo, Cu, Mn and Co molybdates derived from novel precursors catalyze the oxidative dehydrogenation of propane, *Catal. Today*, 107-108(2005), p. 338.

[4] N.V. Lebukhova, V.S. Rudnev, P.G. Chigrin, I.V. Lukiyanchuk, M.A. Pugachevsky, A.Y. Ustinov, E.A. Kirichenko, and T.P. Yarovaya, The nanostructural catalytic composition $CuMoO_4/TiO_2 + SiO_2/Ti$ for combustion of diesel soot, *Surf. Coat. Technol.*, 231(2013), p. 144.

[5] M. Najafi, A. Abbasi, M. Masteri-Farahani, and V.H. Nunes Rodrigues, Synthesis, characterization and crystal structure of a copper molybdate coordination polymer as an epoxidation catalyst, *Inorg. Chim. Acta*, 433(2015), p. 21.

[6] M. Wiesmann, H. Ehrenberg, G. Miehe, T. Peun, H. Weitzel, and H. Fuess, *p–T* phase diagram of $CuMoO_4$, *J. Solid State Chem.*, 132(1997), No. 1, p. 88.

[7] H. Ehrenberg, H. Weitzel, H. Paulus, M. Wiesmann, G. Wltschek, M. Geselle, and H. Fuess, Crystal structure and magnetic properties of $CuMoO_4$ at low temperature (γ-phase), *J. Phys. Chem. Solids*, 58(1997), No. 1, p. 153.

[8] I. Yanase, T. Mizuno, and H. Kobayashi, Structural phase transition and thermochromic behavior of synthesized W-substituted $CuMoO_4$, *Ceram. Int.*, 39(2013), No. 2, p. 2059.

[9] M. Gaudon, C. Carbonera, A.E. Thiry, A. Demourgues, P. Deniard, C. Payen, J.F. Létard, and S. Jobic, Adaptable thermochromism in the $CuMo_{1-x}W_xO_4$ series ($0 \le x < 0.1$): a behavior related to a first-order phase transition with a transition temperature depending on *x*, *Inorg. Chem.*, 46(2007), No. 24, p. 10200.

[10] D. Rathore, R. Kurchania, and R.K. Pandey, Influence of particle size and temperature on the dielectric properties of $CoFe_2O_4$ nanoparticles, *Int. J. Miner. Metall. Mater.*, 21(2014), No. 4, p. 408.

[11] B. Ebin, E. Arıg, B. Özkal, and S. Gürmen, Production and characterization of ZnO nanoparticles and porous particles by ultrasonic spray pyrolysis using a zinc nitrate precursor, *Int. J. Miner. Metall. Mater.*, 19(2012), No. 7, p. 651.

[12] P. Yuan, C. Fan, G. Ding, Y. Wang, and X. Zhang, Preparation and photocatalytic properties of ilmenite $NiTiO_3$ powders for degradation of humic acid in water, *Int. J. Miner. Metall. Mater.*, 19(2012), No. 4, p. 372.

[13] F. Abbas, J. Iqbal, T. Jan, N. Badshah, Q. Mansoor, and M. Ismail, Structural, morphological, Raman, optical, magnetic, and antibacterial characteristics of $CeO_2$ nanostructures, *Int. J. Miner. Metall. Mater.*, 23(2016), No. 1, p. 102.

[14] K. Polak, M. Nikl, K. Nitsch, M. Kobayashi, M. Ishii, Y. Usuki, and O. Jarolimek, The blue luminescence of $PbWO_4$ single crystals, *J. Lumin.*, 72-74(1997), p. 781.

[15] C.S. Lim, Microwave-assisted synthesis and photoluminescence of $MMoO_4$ (M=Ca, Ba) particles via a metathetic reaction, *J. Lumin.*, 132(2012), No. 7, p. 1774.

[16] J.W. Yoon, J.H. Ryu, and K.B. Shim, Photoluminescence in nanocrystalline $MMoO_4$ (M = Ca, Ba) synthesized by a polymerized complex method, *Mater. Sci. Eng. B*, 127(2006), No. 2-3, p. 154.

[17] J.C. Sczancoski, L.S. Cavalcante, N.L. Marana, R.O. da Silva, R.L. Tranquilin, M.R. Joya, P.S. Pizani, J.A. Varela, J.R. Sambrano, M. Siu Li, E. Longo, and J. Andrés, Electronic structure and optical properties of $BaMoO_4$ powders, *Curr. Appl. Phys.*, 10(2010), No. 2, p. 614.

[18] G.J. Xing, R. Liu, C. Zhao, Y.L. Li, Y. Wang, and G.M. Wu, Photoluminescence and photocatalytic properties of uniform $PbMoO_4$ polyhedral crystals synthesized by microemulsion-based solvothermal method, *Ceram. Int.*, 37(2011), No. 7, p. 2951.

[19] X. Wu, J. Du, H. Li, M. Zhang, B. Xi, H. Fan, Y. Zhu, and Y. Qian, Aqueous mineralization process to synthesize uniform shuttle-like $BaMoO_4$ microcrystals at room temperature, *J. Solid State Chem.*, 180(2007), No. 11, p. 3288.

[20] A.B. Campos, A.Z. Simões, E. Longo, J.A. Varela, V.M. Longo, A.T. de Figueredo, F.S. De Vicente, and A.C. Hernandes, Mechanisms behind blue, green, and red photoluminescence emissions in $CaWO_4$ and $CaMoO_4$ powders, *Appl. Phys. Lett.*, 91(2007), art. No. 051923.

[21] Md. Amir, A. Baykal, S. Güner, M. Sertkol, H. Sözeri, and M. Toprak, Synthesis and characterization of $Co_xZn_{1-x}AlFeO_4$ nanoparticles, *J. Inorg. Organomet. Polym. Mater.*, 25(2015), No. 4, p. 747.

[22] Y. Bai, L. Lu, and J. Bao, Synthesis and characterization of lanthanum zirconate nanocrystals doped with iron ions by a salt-assistant combustion method, *J. Inorg. Organomet. Polym. Mater.*, 21(2011), No. 3, p. 590.

[23] H. Zhang, X. Jia, Z. Liu, and Z. Li, The low temperature preparation of nanocrystalline $MgAl_2O_4$ spinel by citrate sol-gel process, *Mater. Lett.*, 58(2004), No. 10, p. 1625.

[24] S. Vivekanandhan, M. Venkateswarlu, and N. Satyanarayana, Novel urea assisted polymeric citrate route for the synthesis of nanocrystalline spinel $LiMn_2O_4$ powders, *J. Alloys Compd.*,

441(2007), No. 1-2, p. 284.

[25] M. Sivakumar, S. Kanagesan, K. Chinnaraj, R. Suresh Babu, and S. Nithiyanantham, Synthesis, Characterization and effects of citric acid and PVA on magnetic properties of $CoFe_2O_4$, *J. Inorg. Organomet. Polym. Mater.*, 23(2013), No. 2, p. 439.

[26] M. Gharagozlou, Synthesis, characterization and influence of calcination temperature on magnetic properties of nanocrystalline spinel Co-ferrite prepared by polymeric precursor method, *J. Alloys Compd.*, 486(2009), No. 1-2, p. 660.

[27] S. Ramaswamy, M. Umadevi, R.K. Rajaram, and V. Ramakrishnan, Infrared and Raman spectral studies of L-ornithine nitrate, *J. Raman Spectrosc.*, 34(2003), No. 10, p. 806.

[28] D. Klissurski, R. Iordanova, M. Milanova, D. Radev, and S. Vassilev, Mechanochemically assisted synthesis of Cu(II) molybdate, *CR Acad. Bulgare Sci.*, 56(2003), No. 8, p. 39.